# Nonstationary phase estimation: A tool for seismic interpretation?

Mirko van der Baan, University of Alberta
Sergey Fomel, University of Texas at Austin
Mike Perz, Arcis Corporation

Spectral decomposition is a standard tool in seismic interpretation to highlight variations in layer thicknesses (e.g., in sand channels and turbidites). This is done by examining changes in peak frequencies in extracted horizon slices (Partyka et al., 1999). Variations in peak frequencies occur due to constructive interference between reflections from the top and bottom of a layer, with lower peak frequencies indicating thicker layers.

In this paper, we argue that a local phase analysis serves as a complementary aid in seismic interpretation because the layer thickness, type of impedance contrast, and boundary shape determine the amplitude, peak frequency and phase of the locally observed wavelet.

## Introduction

Phase mismatches sometimes occur between final processed seismic sections and zero-phase synthetics based on well logs, despite the best efforts for controlled-phase acquisition and processing (Trantham, 1994). Knowledge of the wavelet character and phase is nonetheless important since any phase ambiguities may result in incorrect identification of low- and high-impedance layers in a seismic section (Brown, 2004). For instance, a positive reflection amplitude may correspond to a positive impedance contrast in one part of a section and to a negative impedance contrast in another part in the case of spatially and temporally nonstationary wavelets. The latter example is obviously a worst-case scenario requiring phase changes in excess of 90°; yet temporal phase variations in excess of 60° have been observed (Van der Baan, 2008).

Well logs are, therefore, often used for the estimation of seismic wavelets. The phase is obtained by forcing a well-derived synthetic to match the seismic data, thus assuming the well log provides ground truth. Irrespective of the validity of this approach, well logs are not always available, nor are they always accurate; moreover, different wells can predict different phase corrections, or the phase mismatch can vary with time. Statistical wavelet-estimation methods do not require well logs and analyze the seismic data directly. This leads to greater flexibility and allows us for instance to analyze whether spatial and/or temporal variations occur in the amplitude and phase spectrum of the seismic wavelet.

Edgar and Van der Baan (2009) analyze three marine data sets and find a close similarity between statistical wavelet estimates obtained directly from the data and deterministic wavelets resulting from seismic-to-well ties. Their work gives us confidence in the reliability of statistical wavelet estimates. We explore here another possible application of phase estimation; namely, can it be employed as an aid in seismic interpretation by highlighting areas of potential interest?

## Wavelet types

Before embarking on the main topic of this paper, let us clarify what types of wavelets we are pursuing in the different applications of wavelet phase estimation. We therefore first propose some definitions:

- *The raw or near-surface wavelet:* This is the source wavelet convolved with all near-surface effects including instrument response, ground coupling, the effects of weathering layers, etc. Both surface-consistent deconvolution in land processing and debubbling corrections in marine processing are aimed at collapsing this wavelet.
- *The propagating wavelet:* The physical wavelet that propagates through the Earth, thereby sampling the geology. This wavelet is subject to geometric spreading, apparent and intrinsic attenuation (e.g., due to stratigraphic filtering and multiple scattering) and concomitant dispersion. Both seismic-to-well ties and studies of local attenuation aim to retrieve this wavelet.
- *The locally observed wavelet:* This is the wavelet as observed at a certain point in space and time. Its immediate shape is determined by the local geology such as layer thickness, impedance variations, and boundary shapes, and the current shape of the propagating wavelet. For instance, in the case of a single isolated interface, the shape of the observed wavelet is identical to that of the propagating wavelet, but it is subjected to a 90° phase rotation in the case of a thin high-velocity layer due to interference of the top and bottom reflections (Zeng and Backus, 2005). By contrast, an irregular sequence of thin beds of varying thicknesses is unlikely to display the same characteristic response. Analysis of this local wavelet may thus serve as an aid in seismic interpretation because its shape and phase are determined by the local reflectivity.

## Causes of wavelet variations

Broadly speaking, variations in any of the above wavelets are induced by acquisition, processing and the deterministic physical laws governing wave propagation. We will ignore acquisition effects, despite their important role (Trantham, 1994).

A large variety of processing algorithms exist with an immediate impact on the raw and/or propagating wavelet and its phase (e.g., spiking deconvolution, inverse Q filtering). Imperfect assumptions at various stages in production processing can abruptly modify the phase from one processing stage to the next. Indeed both service companies and operators routinely employ phase analysis as a quality control measure to detect unwanted phase perturbations early in processing.

Wavelet shape is finally determined also by the physical

laws related to wave motion. These affect both the long-term variations in the propagating wavelet (e.g., due to attenuation), and the short-term changes in the locally observed wavelet (because of variations in the local reflectivity series and superposed reflections). Analysis of the character of both the propagating and locally observed wavelets can therefore reveal much information about the underlying causes for their detected variations.

For instance, knowledge of the shape of the propagating wavelet is important to correctly identify positive and negative impedance contrasts in seismic data (Brown, 2004), whereas the locally observed wavelet contains pertinent information on the local reflectivity. Rapid variations in the locally observed wavelet are likely linked to subtle variations in the local geology (e.g., fine-scale layering or the presence of a wedge of varying thickness). In all cases, correct estimation of both the propagating and locally observed wavelet requires robust wavelet-estimation techniques.

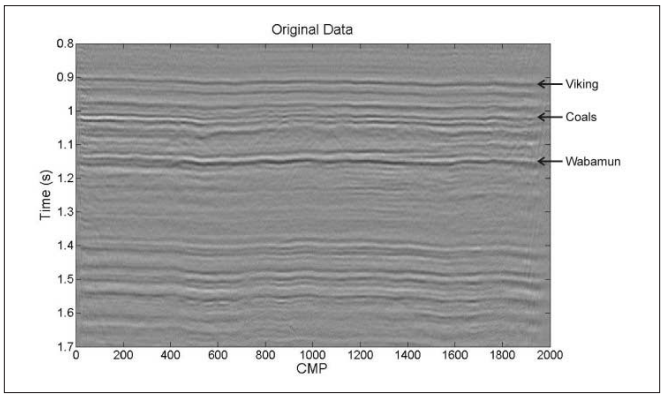


***Figure 1.*** *Data set 1. Migrated section. Viking at 0.9 s, Wabamun at 1.15 s, and coal layers around 1.02 s. The area below 1.4 s shows considerable variation in both wavelet character, frequency content, and reflector strength. This is attributed to the stratigraphic filtering induced by transmission through the coal layers (Perz, 2001). The horizontal axis spans 20 km.*

## Wavelet estimation techniques

The theory and practice of seismic-to-well tying is well established (White et al., 1988; White and Simm, 2003). It is a commonly employed method to estimate seismic wavelets from final processed sections. Yet well logs can produce only rather localized wavelet estimates, and are therefore less suitable for our purpose.

Statistical wavelet-estimation methods do not require well logs and analyze the seismic data directly by means of higher-order statistics. One such technique is kurtosis maximization by constant-phase rotation. The kurtosis is a statistic that measures deviation from non-Gaussianity. If we assume that the seismic wavelet can be described adequately by a frequency-dependent amplitude spectrum but a constant phase, then the phase can be found by phase rotating the seismic data until they become maximally non-Gaussian (Van der Baan, 2008, and references therein). The constant-phase assumption seems to hold in practice except for dispersive wavelets (Van der Baan and Pham, 2008).

Van der Baan and Fomel (2009) recently improved the robustness of this method by employing local attributes (Fomel, 2007a), based on a regularized least-squares optimization across the entire seismic section (Fomel, 2007b). This allows the analysis of spatially and temporally more localized phase variations such that the resulting technique can be used for zero-phasing seismic data, and also as an analysis tool for detecting subtle stratigraphic features in the local geology or for detecting temporal and/or spatial variations in the propagating wavelet.

## Analysis of wavelet character

The enhanced robustness of the statistical wavelet-estimation tools permits us to pursue two complementary applications by simply varying the temporal regularization length. The statistical tools can be utilized for nonstationary estimation of (1) the propagating wavelet by using long temporal regularization lengths and (2) the locally observed phase via short regularization lengths. The underlying assumption is that, for a long regularization length, the geology will be white to first order. Hence, variations in the locally observed wavelets will average out, thereby revealing the propagating wavelet. Conversely, the use of short regularization lengths allows us to focus entirely on the locally observed wavelet.

Here we focus on analysis of the locally observed wavelet and therefore use spatial regularization lengths of the order of 5–25 traces and temporal lengths between 80 and 200 ms. For analysis of the propagating wavelet, we recommend significantly larger spatial and temporal lengths of, respectively, 100 traces and 500 ms or more.

## Case studies

We consider three data sets, all from Canadian sedimentary basins.

*Data set 1.* These data come from the Western Canadian Sedimentary Basin and are also analyzed in Perz (2001). The data set is known to display unusually large variations in both local frequency content and local phase, particularly below a sequence of coal layers.

There are two regional markers in this data set, the Viking at 0.9 s and the Wabamun at 1.15 s (Figure 1). In between these two markers is a coal layer (approximately 1.02 s). Both the Viking and Wabamun are strong continuous markers in most areas; yet in this data set, the Wabamun seems to bifurcate twice, around CMPs 400 and 1300.

Perz analyzes the influence of the coal layers on the Wabamun and deeper reflections with a variety of approaches including numerical modeling using existing well logs, and time-frequency analysis applied to the data. He notes that the data area around CMPs 400–500 constitutes a transitional area in its below-coal characteristics compared with data areas immediately on the left (CMPs 100–400) and right (500–600). He postulates that lateral heterogeneity in the coals is inducing a differential imprint in stratigraphic filtering, which in turn is responsible for the observed character changes in the seismic section.

Stratigraphic filtering results from the highly fluctuating

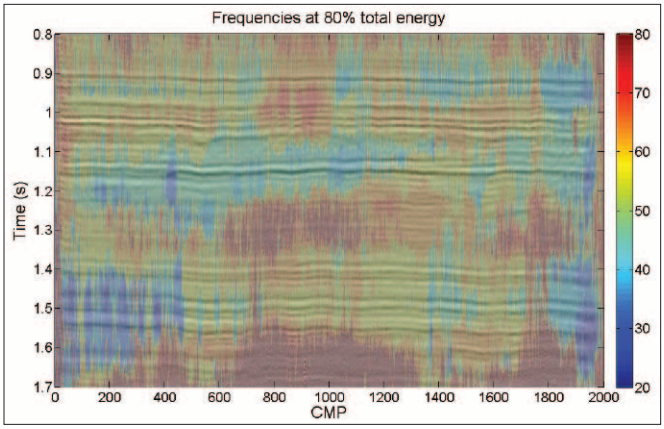


***Figure 2.*** *Data set 1. Frequencies where the cumulative energy is at 80% of the total energy. The Wabamun reflection (at 1.15 s) is characterized by a lower frequency content than the overlying coal layers, indicative of the strong stratigraphic filtering induced by the coals. The left and right edges below 1.4 s are also characterized by very low frequencies, whereas the high frequencies in the central bottom part are due to progressively increasing high-frequency noise.*

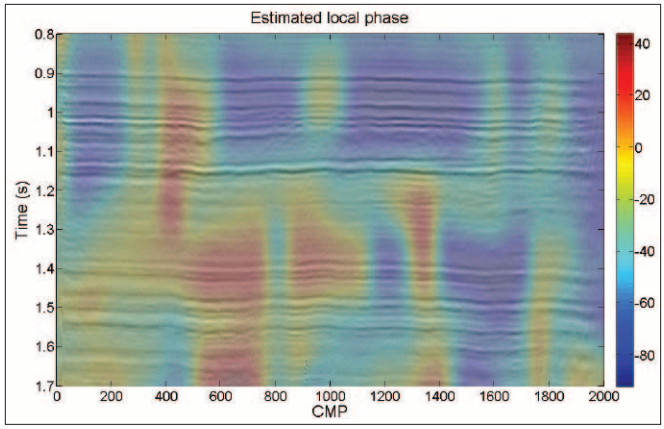


***Figure 3.*** *Data set 1. Extracted local phase using regularization parameters of 50 traces and 50 ms. Large variations in phase occur throughout the seismic section, highlighting changes in reflection character. This happens for instance in CMPs 100–450 and 450–600 below the coal layers (1.3–1.6 s) but also below the apparent bifurcation in the Wabamun at CMP 1300, where reflections depict a stronger reverberative character compared with adjacent CMPs.*

velocity and density profiles within the coal sequence. This leads to frequency-dependent transmissivity that varies with the spatial location (Perz). It has the effect of modifying the propagating wavelet upon passage through the coals through the creation of more or less severe peg-leg multiples following the primary pulse, thereby explaining the apparent bifurcations in the Wabamun reflector at CMPs 400 and 1300. Variation in the coal layering also affects the locally observed wavelet due to tuning. We revisit this data set to analyze both its nonstationary frequency and phase behavior.

Frequency-dependent tuning effects are often analyzed using spectral decomposition in order to detect variations in turbidite layers or meandering channels (Partyka et al.). We analyze the local frequency content using a similar attribute as employed by Perz. We apply a local short-time Fourier transform to all traces, and compute the frequency where the cumulative energy is at 80% of the total energy. Low-frequency values for this cumulative energy criterion indicate larger amounts of attenuation, whereas high frequency values imply small energy losses and a broader spectrum. Note that Perz computes the cumulative amplitude percentile instead of energy. Hence our results are somewhat different but the conclusions remain.

Figure 2 displays the resulting 80% cumulative energy percentiles for each individual trace using a sliding time window of 200 ms. The technique highlights many variations in local frequency content; for instance, in a gross sense, the coal layers at 1 s are characterized by a broader spectrum than the underlying Wabamun (1.15 s). This clearly points to the stratigraphic filtering induced by the rapidly varying density and velocity profiles in the coals.

A more detailed examination of the attribute also reveals a marked difference in character in the section below 1.4 s at CMPs 1–400 compared to the corresponding data at CMPs 400–1200, with the leftmost CMPs displaying significantly lower frequencies than the latter CMPs. Note that this cumulative energy-based attribute does not reveal any variations within CMPs 400–1200 for times 1.4–1.6 s, even though reflections are visibly undulating, in correlation with a similar topography on the Wabamun.

Figure 3 shows the estimated phase of the locally observed wavelet obtained using the approach of Van der Baan and Fomel with a regularization window of 50 traces by 50 ms. This choice for the window size is aimed at resolving the locally observed wavelet as opposed to the propagating one. Clearly the extracted wavelet shows significant temporal and lateral variation. Several observed phase changes coincide with areas depicting visual variations in reflection character.

In general, the Wabamun reflection separates a more homogeneous top area from a more heterogeneous bottom one, although some lateral variations occur above the Wabamun with the strongest between CMPs 400–600. Indeed, the character of the coal layers seems to change around CMP 600 with weaker reflections between CMPs 600–800. Phase analysis reveals a positive phase angle in the coal layers between CMPs 400–600, and a negative angle between CMPs 600–900, thus coinciding with the change in reflection character occurring between these two segments.

In agreement with the cumulative energy attribute (Figure 2), the local phase analysis reveals that the area below the coal layers (1.4–1.7 s) between CMPs 400–600 forms a transitional area between the adjacent CMPs; yet in contrast to the energy attribute, the area between CMPs 600–1200 is divided into several subareas related to the peaks and troughs in the undulating reflections (Figure 3).

Both the spectral and phase analysis also indicate that the reflection character below the apparent bifurcation in the Wabamun at CMP 1300 stands out from the adjacent CMPs. It has somewhat higher frequencies and a different phase of 40°.

Local phase analysis thus produces both similarities and differences compared with a spectral analysis, and therefore serves as a complementary analysis tool. In this case, we can suspect that the propagating wavelet exhibits marked

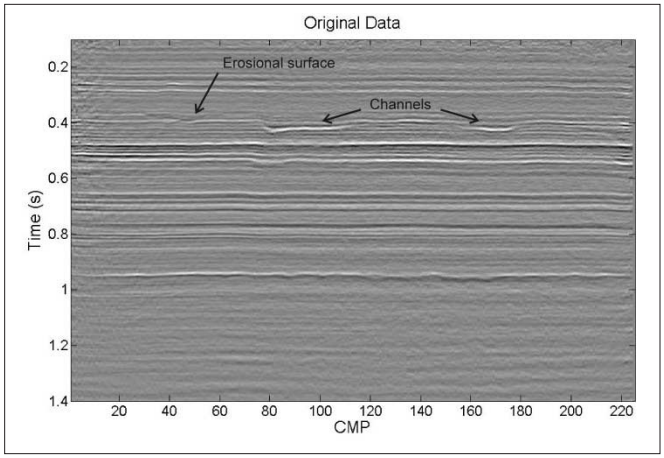


***Figure 4.*** *Data set 2. Migrated section. This line intersects a Cretaceous channel twice, between CMPs 75–105 and 160–180 at 0.40 s. The data show several bands composed of either more tightly or widely spaced reflections. Little stratigraphic filtering is anticipated. Variations in the propagating wavelet are therefore significantly less dramatic than in the previous data set, and short-time variations in both the local frequency content and phase can thus be attributed entirely to the locally observed wavelet. The horizontal axis spans 5.6 km.*

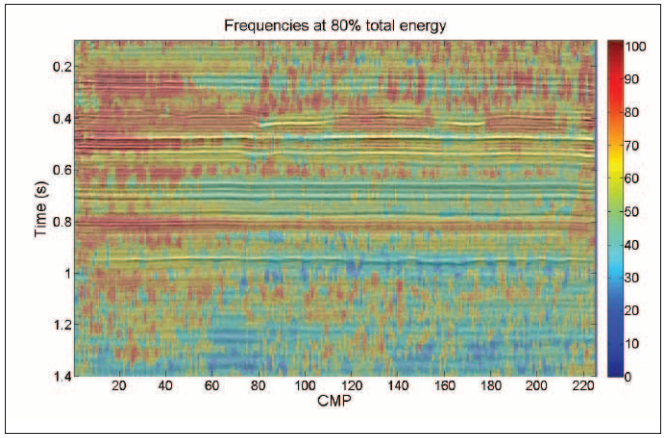


***Figure 5.*** *Data set 2. Frequencies where the cumulative energy is at 80% of the total energy. This display was generated using a short-time Fourier transform with a window length of 150 ms. The frequency attribute divides the data into mostly horizontal bands of alternating high and low frequencies, associated with the more tightly or widely spaced reflections. There is also a general lowering of frequency content with time, indicative of attenuation. Most interestingly, the spectral attribute visibly delineates the channels at 0.40 s which are characterized by lower frequency content due to their increased thickness.*

changes both laterally and vertically because of lateral changes in stratigraphic filtering effects induced by the coals. In addition, the data show that the geology changes laterally as well, both above and below the coals. Although the parameterization for our phase analysis is explicitly keyed to detecting changes in the geology and the locally observed wavelet through the use of small time gates, it is hard to achieve a clear-cut separation of changes in the propagating wavelet (and thus long-term geologic effects related to stratigraphic filtering) and the locally observed wavelet (i.e., the most immediate reflectivity, layer thicknesses and impedance contrasts) in this case. There is evidence of the changes in the propagating wavelet in spite of our choice of parameterization. Yet a combined analysis of local frequency content and phase can reveal many subtle geologic features in complex geologic environments as demonstrated by this data set.

*Data set 2.* The second example also comes from a sedimentary basin in Canada (Figure 4). It contains a Cretaceous meandering channel at 0.42 s that is intersected twice at CMPs 75–105 and 160–180 in this 2D cross section. Above this channel is an erosional surface located between 0.35 (middle portion) and 0.4 s (leftmost CMPs). It is best visible at CMPs 35–50.

Visual inspection of Figure 4 reveals that there are bands of alternating high-frequency areas with tightly spaced reflections and low-frequency regions which are mostly composed of blank intervals without much reflected energy. This is also seen in a display of the frequency values for the 80% cumulative energy percentiles (Figure 5). It identifies the high-frequency intervals between 0.4–0.5 s and around 0.8 s from the surrounding low-frequency ones. Both channel intersections exhibit significantly lower frequency content due to their increased thickness, causing constructive interference in the low-frequency components (Partyka et al.).

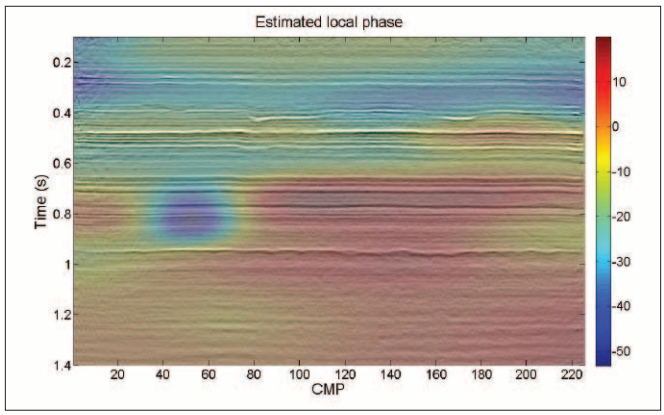


***Figure 6.*** *Data set 2. Extracted local phase using regularization parameters of 20 traces and 100 ms. The local phase analysis yields a significantly more uniform picture than that provided by the spectral analysis (Figure 5). The erosional surface and channel cross sections mark the transition between negative local phase values above and a thin but effectively zero-phase area below (centered on the strong reflection at 0.5 s). Below 0.7 s the local phase is relatively uniform except for the anomalous region at 0.8 s and CMPs 40–60.*

Figure 4 also contains evidence of migration artifacts (smiles). This is most visible at the left edge in particular at shallow times between 0.1 and 0.6 s. These artifacts have introduced high-frequency components, thereby biasing the outcome of the cumulative energy attribute at CMPs 10–45 between 0.2 and 0.6 s in Figure 5. For instance, the visibly low-frequency zone around 0.25 s is identified as a high-frequency area by the cumulative energy attribute at CMPs 10–45. It is therefore important to scrutinize data carefully for the presence of both low- and high-frequency noise before attempting an analysis of local frequency content, (e.g., to identify variations in channel thicknesses).

Figure 6 displays the results of the local phase analysis

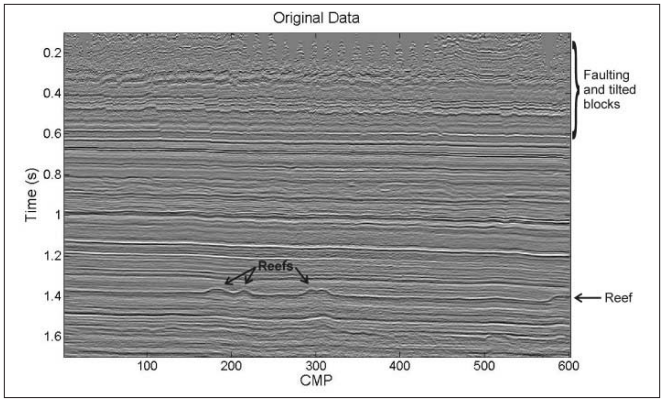


***Figure 7.*** *Data set 3. Migrated section. Note the strong faulting and tilted blocks above 0.5 s and the Devonian reefs at 1.4 s. The latter are producing reservoirs and display possible oil-water contacts. The horizontal axis spans 9 km.*

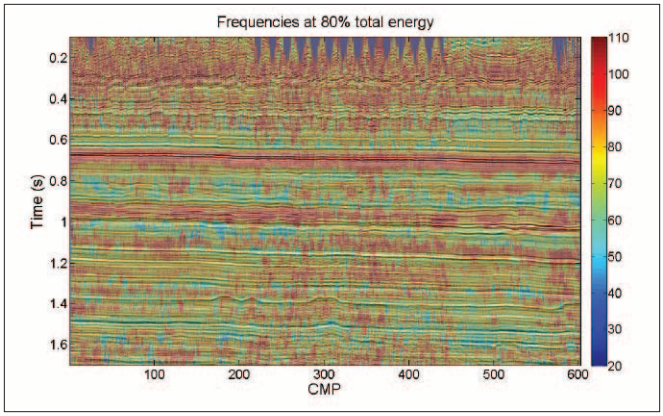


***Figure 8.*** *Data set 3. Frequencies where the cumulative energy is at 80% of the total energy. The time-frequency analysis identifies the high-frequency zones in the upper 0.3 s, around 0.65 s, and 0.95 s, and the intermittent low-frequency zones. As in Figure 5, these zones correspond to areas with more tightly or widely spaced reflections. No specific features are visible around the reefs (1.4 s).*

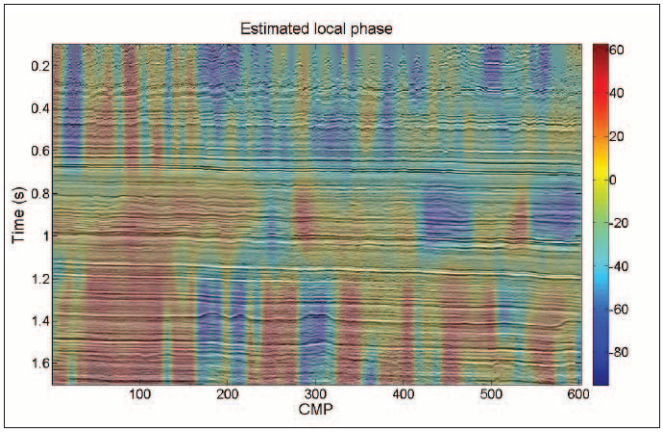


***Figure 9.*** *Data set 3. Extracted local phase using regularization parameters of 5 traces and 100 ms. Large variations in phase occur, displaying a very different picture from Figure 8; in particular, the local phase analysis highlights many of the individual thrust blocks and reefs.*

using regularization lengths of 20 traces and 100 ms. It displays a relatively homogeneous layer between 0.1 and 0.4 s bounded by the erosional surface just above the Cretaceous channel. At 0.4 s the phase changes from –30 to 0° where the section cuts lengthwise through the channel. The phase analysis emphasizes the reflection at 0.5 s giving it approximately a zero phase; it then reverts to the previous local phase of –30° (0.55–0.65 s), before indicating a homogeneous area with an average phase of 10°, with the clear exception of the anomalous area between CMPs 60–80 at 0.8 s. Upon close inspection, the weak double reflection at 0.8 s indeed seems to undergo a phase rotation; except for this area, analysis of the observed wavelet phase indicates a significantly more uniform and layered appearance than the local time-frequency analysis (Figure 5). It also seems to be less influenced by the migration artifacts (half smiles) at the left edge.

Analysis of both the local frequency content and local phase can thus reveal complementary information on the acquired data. In this case, the local frequency attribute better delineates the tightly spaced and reflection-free zones and highlights the presence of the two channel intersections. On the other hand, the local phase analysis seems to be less sensitive here to the presence of high-frequency noise and better demarcates the erosional surface.

*Data set 3.* Our final data set is from the Williston Basin in Saskatchewan. The upper 0.5 s display significant thrust faulting, and there are several Winnipegosis reefs visible at 1.4 s (Figure 7). On close inspection, the largest reefs display possible oil-water contacts. These are known to be producing carbonate reservoirs.

Figure 8 shows the results of the local time-frequency analysis. Roughly speaking, the data are again divided into horizontal bands. The top 0.5 s and the interval from 0.7 to 0.95 s contain relatively high frequencies; in between these high-frequency areas are lower frequency bands often characterized by more widely spaced reflections or even blank areas. Contrary to the meandering channel in the previous example, the spectral decomposition does not highlight any specific variations in features such as reef height, possibly because no clear reflection occurs at the base.

Analysis of the locally observed wavelet produces a different picture. At first sight, the data can be divided into three horizontal bands (0–0.7, 0.7–1.1, and 1.1–1.8 s) with rapid phase variations in particular in the upper and lower bands. In the upper 0.5 s, these variations delineate different blocks of the thrusting and faulting, occurring at either 0.3 or 0.4 s. The phase tool could thus serve as an aid in picking the individual faults.

In the bottom area, the phase variations highlight the three reefs between CMPs 150 and 350. Local phase analysis therefore gives a complementary representation of the data to that obtained through spectral decomposition and may reveal features that otherwise might go unnoticed.

## Discussion

Both the propagating and locally observed wavelets contain much information on the local geology. The propagating

wavelet is affected by in-situ attenuation which depends on sedimentary consolidation, lithology, and even the presence of fluids. In contrast, the amplitude, peak frequency and phase of the locally observed wavelet are determined by the local reflectivity (e.g., layer thickness, type of impedance contrast and boundary shape). Analysis of changes in the local phase along a certain lithological layer can therefore reveal subtle variations in the depositional or erosional history.

Many observed phase changes in all three data sets correspond to areas depicting variations in reflection character. In our interpretation, we attribute short-term variations in estimated phase to changes in the locally observed wavelet and long-term variations to the propagating wavelet, although there is likely to be some ambiguity in this interpretation.

Obviously, a judicious choice of the appropriate window length is a subjective but integral part of the interpretative process, because there is a need to balance the implicitly assumed whiteness of the geology (i.e., absence of correlated geologic processes over long time frames) and anticipated variations in the propagating and/or locally observed wavelets with any inherent bias due to estimation variances.

As a general analysis strategy, we recommend starting with large spatial and temporal regularization lengths spanning the entire data section to determine if the considered section is zero phase. We then generally allow for time-varying wavelets using only temporal regularization lengths of 200–500 ms to investigate whether the data are stationary in the time domain. Finally, we shorten the spatial regularization lengths as well to reveal any spatially and temporal nonstationarity. This procedure is designed to increase our understanding of the data, increasing confidence in our ability to distinguish between the propagating and locally observed wavelets and to recognize any noisy artifacts in the final images.

## Conclusions

Kurtosis maximization by constant phase rotation is a useful tool for nonstationary phase estimation. Statistical phase analysis can be used to extract nonstationary seismic wavelets suitable for deconvolution, as a quality control to check deterministic phase corrections resulting from seismic-to-well ties, and also as an interpretation tool. In the latter case, it can be employed to highlight areas of subtle stratigraphic variations in the local geology (including pinch outs, and variations in turbidite and coal sequences, meandering channels and carbonate reefs) or to "red flag" spatial variations in the character of the propagating wavelet.

We advocate analysis of local phase character as a complementary tool to spectral decomposition for highlighting variations in local reflection characteristics. TLE

## References


Brown, A. R., 2004, Interpretation of three-dimensional seismic data (sixth edition): SEG.

Edgar, J. A. and M. Van der Baan, 2009, How reliable is statistical wavelet estimation?: 71st International Meeting and Convention, EAGE, Extended Abstracts, V003.

Fomel, S., 2007a, Local seismic attributes: Geophysics, **72**, no. 3, A29–A33.

Fomel, S., 2007b, Shaping regularization in geophysical-estimation problems: Geophysics, **72**, no. 2, R29–R36.

Partyka, G., J. Gridley, and J. Lopez, 1999, Interpretational applications of spectral decomposition in reservoir characterization: The Leading Edge, **18**, 353–360.

Perz, M., 2001, Coals and their confounding effects: CSEG Recorder, **26**, no. 12, 34–53.

Trantham, E. C., 1994, Controlled-phase acquisition and processing: 64th Annual International Meeting, SEG, Expanded Abstracts, 890–894.

Van der Baan, M., 2008, Time-varying wavelet estimation and deconvolution by kurtosis maximization: Geophysics, **73**, no. 2, V11–V18.

Van der Baan, M. and S. Fomel, 2009, Nonstationary phase estimation using regularized local kurtosis maximization: Geophysics, **74**, no. 6, A75–A80.

Van der Baan, M. and D. -T. Pham, 2008, Robust wavelet estimation and blind deconvolution of noisy surface seismics: Geophysics, **73**, no. 5, V37–V46.

White R. E. and R. Simm, 2003, Good practice in well ties: First Break, **21**, no. 10, 75–83.

White R. E., R. Simm, and S. Xu, 1998, Well tie, fluid substitution and AVO modeling: a North Sea example: Geophysical Prospecting, **46**, 323–346.

Zeng, H., and M. M. Backus, 2005, Interpretive advantages of 90°-phase wavelets. Part 1: Modeling: Geophysics, **70**, no. 3, C7–C15.


*Acknowledgments: We are grateful to an anonymous company, Encana, and Petrobank for permission to use and show the data. We thank Satinder Chopra, Don Herron, and Alan Jackson for their constructive feedback on the original text. MvdB also thanks the sponsors of the project Blind Identification of Seismic Signals for financial support.*

*Corresponding author: Mirko.vanderBaan@ualberta.ca*